TRENDS IN SCIENCES 2025; 22(12): 11043
https://doi.org/10.48048/tis.2025.11043 RESEARCH ARTICLE

The Influence of Yttrium Doping on The Microstructure and Magnetic Properties of Barium Hexaferrite

Nazaruddin Nasution[1], Syahrul Humaidi[1,*], Erna Frida[1], Tulus Na Duma[1], Phahul Zhemas Zul Nehan[2], Marzuki Naibaho[2,3] and Masno Ginting[3]

[1]Postgraduate Program (Physics), Fakultas Matematika Dan Ilmu Pengetahuan Alam, Universitas Sumatera Utara, Medan 20155, Indonesia
[2]Study Program of Materials Science, Department of Physics, Faculty of Mathematics and Natural Science, Universitas Indonesia, Depok 16424, Indonesia
[3]Center for Advanced Materials Research (PRMM) - National Research and Innovation Agency (BRIN), Tangerang-South, Banten 15314, Indonesia

([*]Corresponding author's e-mail: syahrul1@usu.ac.id)

Received: 24 June 2025, Revised: 2 July 2025, Accepted: 9 July 2025, Published: 30 August 2025

Abstract

This study investigates the effect of Yttrium (Y) addition as a doping element on the microstructure and magnetic properties of barium hexaferrite ($BaFe_{12}O_{19}$), synthesized using the High Energy Milling (HEM) method. Samples with varying Y concentrations (x = 0.00, 0.05, 0.1 and 0.15) were prepared and characterized using X-ray Diffraction (XRD), Scanning Electron Microscope-Energy Dispersive X-ray (SEM-EDX), and Vibrating Sample Magnetometer (VSM). The XRD results showed that all samples exhibited a hexagonal M-type crystal structure with a P63/mmc space group. The addition of Y caused a shift in diffraction peaks toward lower angles, indicating an increase in lattice parameters. SEM morphological analysis revealed a decrease in grain size (D_{SEM}) with increasing Y content, from 813 nm (x = 0) to 519 nm (x = 0.15). Additionally, magnetic measurements indicated that the sample with x = 0.05 (Y5) had the optimal magnetic properties, with a saturation magnetization (M_S) of 58.11 emu/g and a coercivity (H_C) of 2,715 Oe, making it a promising candidate for microwave absorber applications. This study demonstrates that Y doping can modify the structure and enhance the magnetic properties of barium hexaferrite, particularly in optimizing magnetization and reducing coercivity for microwave absorption applications.

Keywords: $BaFe_{12}O_{19}$, High energy milling, Magnetic properties, Microwave absober properties, Yttrium doping

Introduction

Magnetic materials have made a significant contribution to the advancement of electronic information technology and manufacturing. One of the technological developments is microwave absorber materials, which aim to (i) reduce electromagnetic wave radiation from electronic devices that may negatively affect human health in the long term, and (ii) enhance stealth radar technology in the military sector [1,2]. Various magnetic materials have been explored to support these applications, including metal oxides, spinel ferrites, hexaferrites, perovskite manganites, magnetic alloys, and 2D materials [3-6]. Among these materials, hexaferrites present both scientific and technical advantages. These are attributed to their characteristics, such as high Curie temperature, high saturation magnetization, high coercivity, low eddy current losses, high electrical resistivity, excellent corrosion resistance, good chemical stability, low material cost, and ease of production [7-12]. The general formula for M-type hexaferrite with a magnetoplumbite structure is $AFe_{12}O_{19}$, where A can be Ba, Sr, or Pb [4,13-15].

In addition to their role in hexaferrites, the constituent ions Ba^{2+} and Fe^{3+} are known for their functional versatility in other advanced material systems. Barium has been widely used in polymer composites and dielectric materials due to its thermal and electrical properties [16], while Fe^{3+} plays key roles in flexible electronics, catalysis, and energy storage systems because of its redox activity and multifunctionality [17]. M-type hexaferrites are considered highly suitable for industrial-scale microwave absorber applications. This is supported by the fact that M-type hexaferrites currently dominate up to 57% of permanent magnetic materials [2]. Due to their great potential, the development and exploration of M-type hexaferrites remain a central focus in magnetic material research.

The $BaFe_{12}O_{19}$ compound has been extensively studied due to its potential applications, particularly as a microwave absorber. Generally, $BaFe_{12}O_{19}$ has a hexagonal crystal structure containing 64 ions, including both cations and anions, within each unit cell [2]. This crystal structure belongs to the P63/mmc space group, characterized by ions distributed across 11 different symmetry sites. A single unit cell contains 24 Fe^{3+} ions, which are crystallographically located in 3 distinct lattice sites: Tetragonal ($4f_1$), octahedral (12k, 2a and $4f_2$), and trigonal bipyramidal (2b) [11,18]. More specifically, 16 of the Fe^{3+} ions have spins aligned parallel to the crystallographic c-axis, forming the majority spin direction ↑ (12k, 2a and 2b), while the remaining 8 Fe^{3+} ions are aligned in the opposite direction, forming the minority spin direction ↓ ($4f_1$ and $4f_2$) [19]. This unique arrangement allows for the substitution of cations in $BaFe_{12}O_{19}$ with other elements, aiming to enhance its magnetic properties. Such modifications significantly affect its performance in applications like microwave absorbers by altering its electronic structure, resonance frequency, and atomic magnetization [2,4,20]. Therefore, cation substitution in $BaFe_{12}O_{19}$ is a promising strategy for improving its functional properties.

Cation substitution in the $BaFe_{12-x}RE_xO_{19}$ compound, where RE represents rare earth elements such as Y^{3+}, La^{3+}, Gd^{3+}, Ho^{3+}, Er^{3+} and Ce^{3+}, can lead to structural changes. These changes include structural distortion, lattice strain, crystallite size, and grain size, all of which can contribute to improvements in magnetic and electronic properties [2,9,21-25]. Hashhash *et al.* [22] reported a study on cation substitution in the compound $Ba_{0.5}Sr_{0.5}Fe_{11.4}R_{0.6}O_{19}$, where R = La, Yb, Sm, Gd, Er, Eu, and Dy. The results showed that substitution with different rare earth elements, each having varying ionic radii, affected key magnetic parameters such as maximum magnetization (M_{max}), saturation magnetization (M_S), remanent magnetization (M_r), and coercivity (Hc). The highest values of M_{max}, M_S, and M_r under an applied magnetic field of 2 T were observed in the $Ba_{0.5}Sr_{0.5}Yb_{0.6}Fe_{11.4}O_{19}$ compound, with respective values of 59.8, 63.1, and 29.4 emu/g. It was also reported that Yb substitution resulted in the lowest H_C value among the samples, at 2,400 Oe [22]. Similarly, Sanker *et al.* [2] investigated the effect of Yttrium (Y) substitution in $BaFe_{12-x}Y_xO_{19}$ compounds with x = 0.0, 0.2, 0.4 and 0.6. They found that at x = 0.2 with a sintering temperature of 1,100 °C, the highest values of M_{max}, M_S, and M_r were achieved 100.27, 106.00, and 49.86 emu/g, respectively under an applied magnetic field of 2 T. Meanwhile, the H_C value was around 2,389.3 Oe. Based on these 2 studies, it is evident that Y substitution in $BaFe_{12}O_{19}$ compounds can result in higher M_{max}, M_S, and M_r values, along with relatively higher H_C. These characteristics align with some of the essential criteria for effective microwave absorber materials, which include high saturation magnetization and low coercivity [4,5]. Recent research has also highlighted the potential of ferrite-based materials, particularly those doped with rare-earth elements such as Y, for use in electromagnetic applications [26].

In addition to cation substitution, other parameters that significantly affect the structure and magnetic properties of materials include composition, synthesis method, and heat treatment conditions [3,27-30]. This has been confirmed by several previous studies. Sarker *et al.* [2] reported the influence of different heating temperatures on $BaFe_{12-x}Y_xO_{19}$ compounds with x = 0.0, 0.2, 0.4, and 0.6 synthesized by a specific method. They found that increasing the heating temperature tended to enhance the values of M_{max}, Ms, Mr, and Hc. These changes were also related to variations in crystallite size and structural parameters. Rehman *et al.* [24] investigated $BaFe_{12-x}Y_xO_{19}$ compounds (x = 0.0, 0.02, 0.05, 0.08, 0.10 and 0.13) prepared via the solid-state reaction method. Their results showed that the highest M_S value reached 57.135 emu/g, while the lowest H_C

was around 2,165.83 Oe under an applied magnetic field of 1 T. On the other hand, Sharma *et al.* [25] studied $BaFe_{12-x}Y_xO_{19}$ (x = 0.0, 0.1 and 0.2) synthesized through the co-precipitation method, in which they observed variations in magnetic properties. The highest M_S obtained was 59.85 emu/g, and the lowest Hc was 310 Oe. However, the co-precipitation method tended to reduce M_S and increase H_C when Y was used to substitute Fe in the $BaFe_{12-x}Y_xO_{19}$ compounds. Therefore, controlling parameters such as cation substitution, synthesis technique, and thermal treatment is crucial for optimizing the magnetic and electronic properties of hexaferrite materials. A deeper understanding of the interactions among these parameters may open new opportunities for more efficient applications.

Although numerous studies have investigated the substitution of Fe with Y in $BaFe_{12-x}Y_xO_{19}$, there is still limited information regarding the effects of using High Energy Milling (HEM) in the synthesis of this material. HEM was chosen due to several advantages, including its simplicity, low cost, the production of more homogeneous particle sizes, and the avoidance of excessive chemical solvents, which results in minimal waste. Therefore, this study investigates the influence of Y substitution on the structural and magnetic properties of $BaFe_{12-x}Y_xO_{19}$ compounds (x = 0.0, 0.05, 0.1 and 0.15) synthesized using the HEM method. It is expected that HEM may contribute to intrinsic defects and structural modifications that enhance magnetic performance. The aim is to increase the values of M_{max}, M_S, and M_r, while decreasing H_C, as these parameters are crucial for improving the performance of microwave absorber materials.

Materials and methods

M-type barium hexaferrite compounds with the formula $BaFe_{12-x}Y_xO_{19}$ (x = 0.00, 0.05, 0.1 and 0.15) were synthesized using the HEM method. To produce the samples, analytical grade precursors were used, including barium carbonate ($BaCO_3$), iron (III) oxide (Fe_2O_3), and yttrium oxide (Y_2O_3). Sample codes were assigned to simplify identification: Y0 ($BaFe_{12}O_{19}$), Y5 ($BaFe_{11.95}Y_{0.05}O_{19}$), Y10 ($BaFe_{11.9}Y_{0.1}O_{19}$), and Y15 ($BaFe_{11.85}Y_{0.15}O_{19}$). Before starting the synthesis, the precursors were calculated and weighed based on the designed stoichiometry. All weighed precursors were placed in a milling container, and a small amount of ethanol was added. The milling process was carried out for 3 h at room temperature. The resulting wet powder was dried in an oven at 80 °C for 20 h. Then, the dry powder was sintered at 1,200 °C for 3 h. Finally, the sintered powder was ground manually and sieved to a particle size of 200 mesh, making it ready for characterization.

Structural analysis was carried out using X-ray Diffraction (XRD, SMARTLAB Rigaku) with a Cu-Kα radiation source (λ = 1.54056 Å) over a 2θ range of 10° to 90°, with a step width of 0.01°. Furthermore, the XRD measurements were conducted at room temperature using powder samples. The sample morphology was examined using a Scanning Electron Microscope (SEM), while the elemental distribution was analyzed using Energy Dispersive X-ray Spectroscopy (EDX). Both characterizations were performed with a HITACHI-SU3500 SEM-EDX instrument operated at 15 kV. The magnetic properties of the materials were characterized at room temperature using a Vibrating Sample Magnetometer (VSM250, Dexing Magnet Ltd) under an applied magnetic field range of 0 - 1 T.

Results and discussion

The structural properties

Figure 1 presents the XRD patterns of $BaFe_{12-x}Y_xO_{19}$ compounds with x = 0.0, 0.05, 0.1, and 0.15 (M-type hexaferrite, BaM), measured over a 2θ range of 10° - 90°. The measurements were conducted at room temperature using powder samples. Several prominent diffraction peaks indicating the presence of the $BaFe_{12-x}Y_xO_{19}$ phase were observed, appearing at approximately the following 2θ positions: 23.0° (006), 30.3° (110), 30.8° (112), 31.2° (008), 32.1° (107), 34.1° (114), 35.1° (200), 37.1° (203), 40.3° (205), 42.7° (206), 46.5° (10 11), 50.3° (209), 55.3° (217), 57.3° (304), 63.5° (224), 67.3° (20 14), 71.8° (11 16), and 74.1° (403) [2,29]. Furthermore, the inset in **Figure 1** shows a leftward shift of the diffraction peaks with increasing Y concentration, suggesting changes in the structural parameters of the compound. Structural analysis (including crystal structure, lattice parameters, average crystallite size, and theoretical density) was carried out using the Rietveld refinement method with the aid of FullProf software [20,25].

The results of the Rietveld refinement analysis confirmed that all compounds exhibit XRD patterns consistent with the ICSD-16157 reference. **Figure 2** presents all the graphs obtained from the observed Rietveld refinement analysis. All detected peaks validate the formation of a single-phase BaM with a hexagonal crystal structure belonging to the space group P63/mmc [31,32]. In detail, the structural parameters obtained from the Rietveld refinement analysis are summarized in **Table 1**. The lattice parameters indicate that the values of a, b, c, and the lattice volume tend to increase slightly with the substitution of Fe^{3+} ions by Y^{3+} ions. This can be explained by the fact that the ionic radius of Y^{3+} (1.04 Å) is larger than that of Fe^{3+} (0.64 Å), causing a mismatch in the crystal lattice when Y^{3+} ions substitute Fe^{3+} ions, which in turn increases the lattice parameters [2,25,33,34]. In addition, the type of BaM formed can be determined by comparing the lattice parameter ratio c/a within a specific range. Sarker reported that $BaFe_{12-x}Y_xO_{19}$ (x = 0.0, 0.2, 0.4 and 0.6) has c/a values in the range of 3.93 - 3.94 [2]. Wagner reported that M-type $BaGa_{12}O_{19}$ has a c/a ratio of 3.96 [35]. Topkaya also reported that $BaFe_{11.9}Y_{0.1}O_{19}$ has a c/a ratio of 3.936 [9]. Furthermore, Ginting reported that $BaFe_{11.8}Co_{0.1}Ni_{0.1}O_{19}$ has a c/a ratio of 3.95 [6], while $Ba_{0.8}Ca_{0.2}Fe_{12}O_{19}$ has a c/a ratio of 3.92 [36]. For a more complex doping system, $BaCo_1Zr_1Fe_{10}O_{19}$ exhibits a c/a ratio as high as 3.97 [52]. Based on these reports, it can be concluded that M-type barium hexaferrites typically exhibit c/a ratios in the range of 3.92 - 3.97. Therefore, the synthesized $BaFe_{12-x}Y_xO_{19}$ compounds with x = 0.0, 0.05, 0.1, and 0.15 can be classified as M-type barium hexaferrites. As a schematic illustration, the hexagonal crystal structures of the M-type compounds are shown in **Figure 3**.

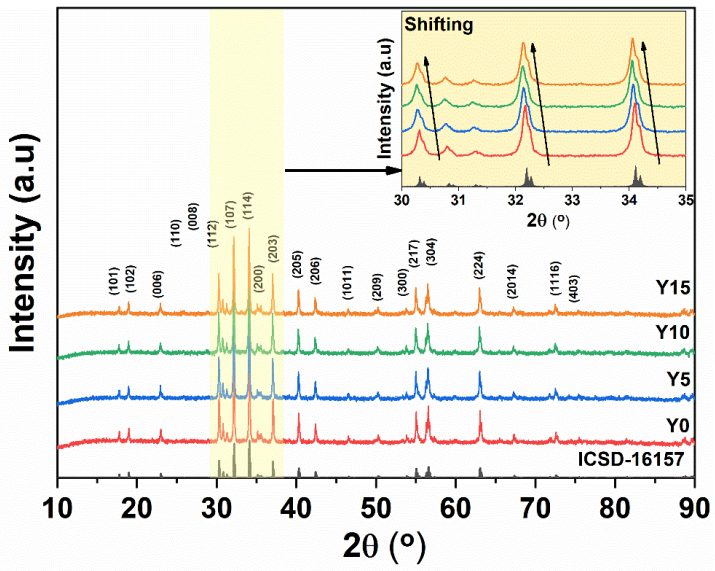

Figure 1 XRD patterns of $BaFe_{12-x}Y_xO_{19}$ compounds with x = 0.0, 0.05, 0.1 and 0.15 in the 2θ range of 10° - 90°, with an inset showing the XRD patterns in the 2θ range of 30° - 35°.

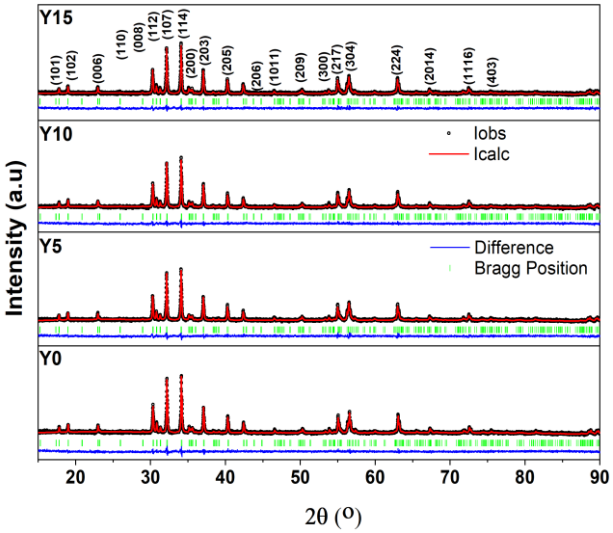

Figure 2 XRD patterns resulting from the Rietveld refinement analysis for $BaFe_{12-x}Y_xO_{19}$ compounds with x = 0.0, 0.05, 0.1, and 0.15, where the black circles represent the experimentally observed XRD data (I_{Obs}), the red line corresponds to the calculated XRD pattern obtained from the Rietveld refinement (I_{Calc}) that matches the experimental data, the blue line indicates the difference between the observed and calculated patterns, and the green vertical lines mark the Bragg reflection positions.

Table 1 Structural parameters obtained from the XRD pattern analysis of $BaFe_{12-x}Y_xO_{19}$ compounds with x = 0.0, 0.05, 0.1, and 0.15.

Structural parameters	**Y0**	**Y5**	**Y10**	**Y15**
Crystal Structure	Hexagonal	Hexagonal	Hexagonal	Hexagonal
Space Group	*P63/mmc*	*P63/mmc*	*P63/mmc*	*P63/mmc*
a = b	5.8918	5.89517	5.8966	5.9001
C	23.2024	23.23104	23.2199	23.2353
c/a	3.9381	3.9407	3.9379	3.9381
V	697.5189	699.1849	699.1822	700.4702
microstrain	0.00042	0.00048	0.00049	0.00047
βcos	0.001696	0.001916	0.001980	0.001862
Σ	0.03569	0.03583	0.03565	0.03568
D_{SC}	87.09	77.83	76.07	80.10
D_{SEM} (nm)	813 ± 283	791 ± 370	620 ± 302	519 ± 259
densitas	5.2930	5.2883	5.2961	5.2942
Chi (%)	1.2800	1.2500	1.2000	1.2000
Rbragg	13.3100	11.9900	12.3400	9.3410

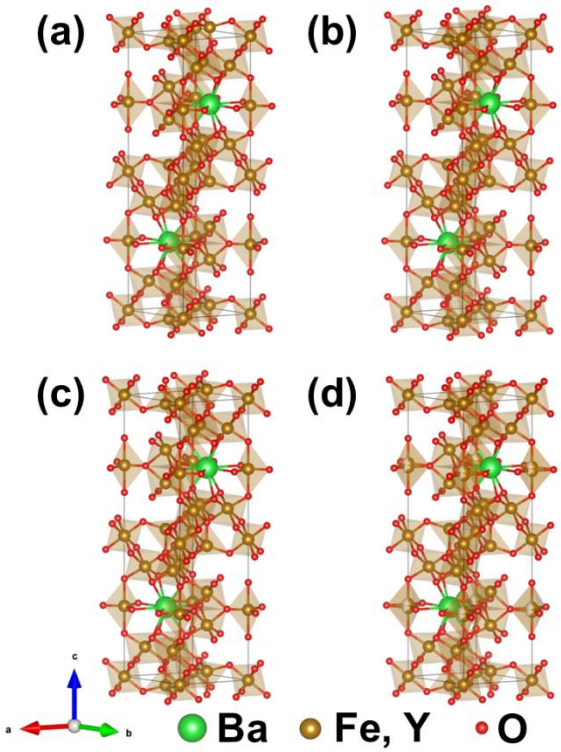

Figure 3 Schematic illustration of the hexagonal crystal structure obtained from the Rietveld refinement of $BaFe_{12-x}Y_xO_{19}$ compounds for (a) x = 0.0, (b) x = 0.05, (c) x = 0.1, and (d) x = 0.15.

The average crystallite size was determined using the Debye-Scherrer equation, which is defined as follows [2,20]:

$$D_{SC} = \frac{k\lambda}{\beta\cos\theta} \quad (1)$$

where, D_{SC} is the average crystallite size, k is the Scherrer constant, λ is the X-ray wavelength, β is the full width at half maximum (FWHM), and θ is the Bragg diffraction angle. The calculated Dsc values, as presented in **Table 1**, show a decreasing trend with increasing substitution concentration of Y ions. The D_{SC} values were found to be in the range of 76.07 - 87.09 nm. This reduction is consistent with the report by Almessiere, which demonstrated that the substitution of Fe with Nb in $BaFe_{12-x}Nb_xO_{19}$ led to a decrease in average crystallite size from 46.1 nm (x = 0) to 33.2 nm (x = 0.1) [37]. This phenomenon is associated with the leftward shift of XRD peaks due to Y ion substitution, as shown in the inset of **Figure 1**. This statement is supported by the report of Marouani, who stated that the leftward shift of XRD peaks may contribute to a reduction in Dsc values [38]. This peak shift is attributed to the larger ionic radius of Y^{3+} compared to Fe^{2+}, which can cause significant changes in various structural parameters. These changes include: (i) a decrease in Fe-O bond length, (ii) alterations in the Fe-O-Fe bond angle and position, and (iii) modifications in the overall dimensions of the crystal unit cell, all of which affect the fundamental properties of the structure [20,38]. These structural changes have a direct impact on the fundamental characteristics of the compound. Furthermore, the crystallite size can be used to calculate the dislocation density (σ) through the relationship $\sigma = 1/D_{SC}^2$. The observed significant reduction in crystallite size likely corresponds to an enhancement in dislocation density within the material [20]. Therefore, the leftward shift in XRD peaks observed in these samples can be well explained by the influence of cation substitution on the structural parameters.

The density of all samples was calculated using data obtained from the Rietveld refinement of X-ray diffraction patterns, according to the following equation [39-41]:

$$\rho_{XRD} = \frac{ZM}{N_A V} \quad (2)$$

where ρ_{XRD} represents the density determined from XRD measurements (g/cm^3), Z is the number of molecules per unit cell, M is the molecular weight (g/mol), N is Avogadro's constant (6.021×10^{23} mol^{-1}), and V is the unit cell volume. The analysis results show that the XRD density values tend to remain stable without significant changes, even though the molar mass of Y^{3+} ions (88.908 a.m.u) is higher than that of Fe^{3+} ions (55.85 a.m.u) [2]. This is due to the very small amount of Fe cation substitution by Y. When compared to the theoretical density of $Ba_{0.5}Sr_{0.5}RE_{0.6}Fe_{11.4}O_{19}$ compounds (RE = La, Yb, Sm, Gd, Er, Eu and Dy), the density of $BaFe_{11.9}Y_{0.1}O_{19}$ was found to be higher than that of $Ba_{0.5}Sr_{0.5}Yb_{0.6}Fe_{11.4}O_{19}$ (ρ_{XRD} = 5.291 g/cm^3). However, for RE substitutions other than Yb, the ρ_{XRD} values of $Ba_{0.5}Sr_{0.5}RE_{0.6}Fe_{11.4}O_{19}$ were higher than that of $BaFe_{11.9}Y_{0.1}O_{19}$, indicating that the $Ba_{0.5}Sr_{0.5}RE_{0.6}Fe_{11.4}O_{19}$ compounds are denser. Additionally, the variation in ρ_{XRD} values correlates with the dislocation density values observed, where no significant change in dislocation density was noted. This phenomenon is consistent with the substitution of Fe by Y in $BaFe_{12-x}Y_xO_{19}$ compounds (with x = 0.0, 0.3, 0.5, 0.7 and 0.9), where increasing x leads to an increase in dislocation density, which in turn decreases the XRD density [20].

The morphological properties

The SEM images of $BaFe_{12-x}Y_xO_{19}$ compounds with x = 0.00, 0.05, 0.10, and 0.15 are shown in **Figure 4**. The surface morphology exhibits irregular grain shapes and sizes. This is clearly evident from the presence of both large and small grains on the surface [42]. The average grain size (D_{SEM}) of each sample was calculated using the ImageJ software. The obtained D_{SEM} values show a decreasing trend with increasing Y concentration. The D_{SEM} values are 813, 791, 620 and 519 nm for Y0, Y5, Y10, and Y15 samples, respectively. More detailed results of the D_{SEM} values can be seen in the histogram shown in **Figure 4** and in **Table 1**. The decrease in D_{SEM} is presumably due to the cation substitution effect by rare-earth ions such as Y^{3+}, which have a different average ionic radius compared to Fe^{3+} ions [37,43]. On the other hand, the presence of Y^{3+} ions, as a rare-earth element, may contribute to the inhibition of grain growth during the heating process [23].

In addition, this study used only 1 synthesis batch for each sample composition. The relatively large standard deviations in grain size values, as shown in **Table 1**, may be caused by variations during the milling and sintering steps. Although the overall trend of decreasing grain size with higher Y content is still clear, the consistency of the High Energy Milling (HEM) method has not been fully evaluated. Future studies are needed to repeat the synthesis process using multiple batches in order to check reproducibility and improve control over particle size. This would help ensure that the relationship between microstructure and magnetic properties is more reliable.

Table 2 The semi-quantitative results from the EDX measurements compared with the stoichiometry.

Sample		Ba (at%)	Fe (at%)	Y (at%)	O (at%)
Y0	Stoichiometry	3.13	37.5	0	59.37
	Experiment	3.35	36.89	0	59.76
Y5	Stoichiometry	3.13	37.35	0.15	59.37
	Experiment	3.58	36.38	0.11	59.93
Y10	Stoichiometry	3.13	37.19	0.31	59.37
	Experiment	3.5	34.46	0.2	61.84
Y15	Stoichiometry	3.13	37.03	0.46	59.38
	Experiment	3.54	36.13	0.07	60.26

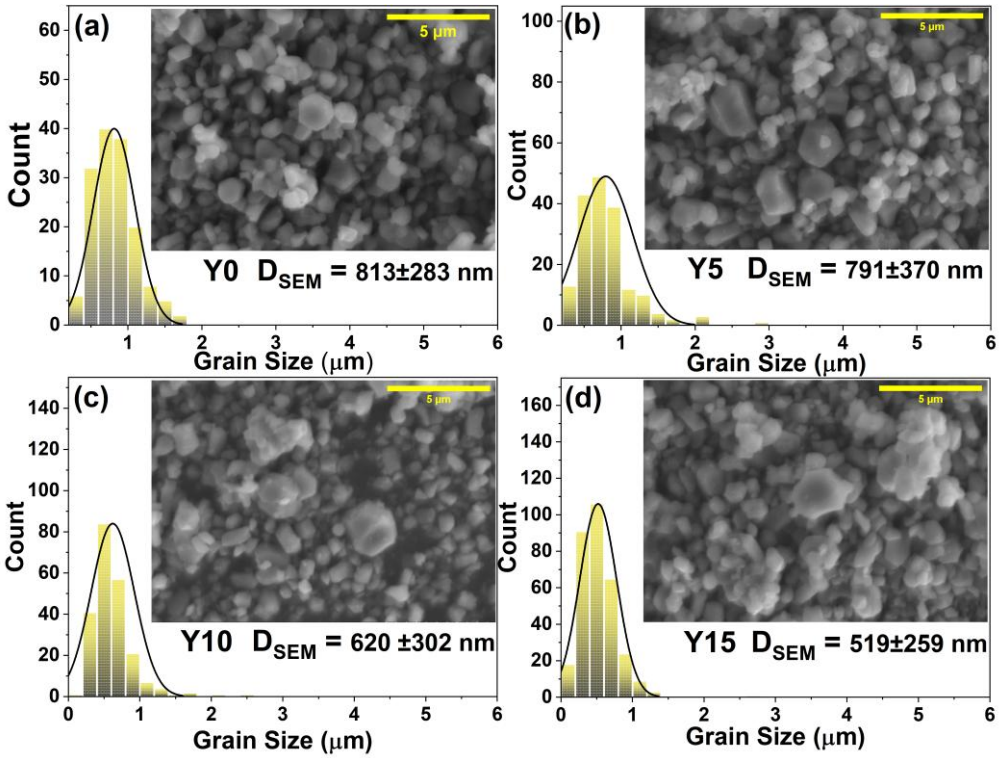

Figure 4 The grain size distribution histogram and inserted SEM micrographs $BaFe_{12-x}Y_xO_{19}$ (a) x = 0.0, (b) x = 0.05, (c) x = 0.1, and (d) x = 0.15 compounds.

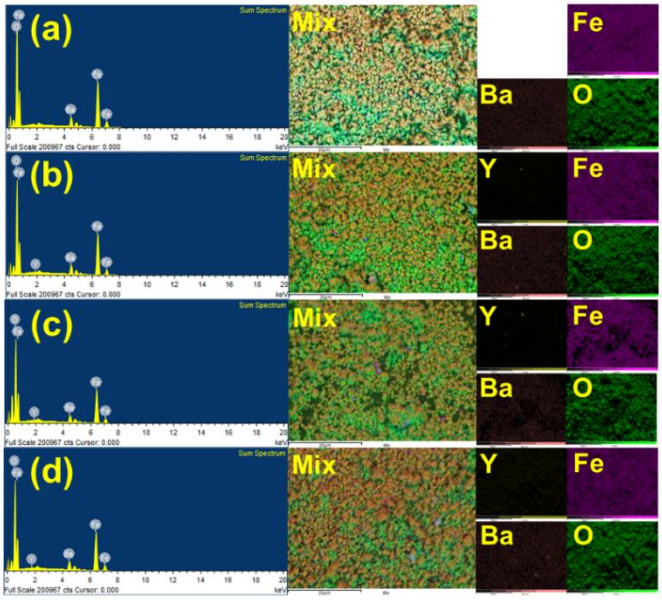

Figure 5 The EDX measurement results in the form of spectral curves and elemental mapping of the $BaFe_{12-x}Y_xO_{19}$ (a) x = 0.0, (b) x = 0.05, (c) x = 0.10, and (d) x = 0.15 compound.

Figure 5 presents the spectrum and elemental mapping results from the EDX measurements for all samples. The spectral curves confirm that the detected elements for the Y0 sample are Ba, Fe, and O, while for the Y5, Y10, and Y15 samples, the detected elements are Ba, Fe, Y, and O. This confirms that the detected elements are consistent with the intended compound [20]. To further validate the synthesized compounds, the atomic percentages of each element in $BaFe_{12-x}Y_xO_{19}$ (x = 0.00, 0.05, 0.10 and 0.15) were compared with the theoretical stoichiometry, as tabulated in **Table 2**. The comparison results further confirm that each synthesized

compound was successfully produced in accordance with its stoichiometry.

Magnetic properties

The magnetic properties of the $BaFe_{12-x}Y_xO_{19}$ compounds (x = 0.0, 0.05, 0.10 and 0.15) were measured using a VSM instrument at room temperature under an applied magnetic field of 10 kOe, as shown in **Figure 6**. The magnetic behavior exhibited is characteristic of hard magnetic materials, indicated by high coercivity and remanent magnetization values, which are typical features of M-type hexaferrites [44-49]. The magnetization of $BaFe_{12-x}Y_xO_{19}$ (x = 0.0, 0.05, 0.10 and 0.15) correlates with the aligned magnetic field, influencing an increase in magnetization values [24]. Based on **Figure 6**, the identifiable magnetic parameters include M_{max}, H_C and M_r. More detailed information regarding these parameters is summarized in **Table 3**. The observed maximum magnetization values were 50.39, 53.23, 49.65, and 47.95 emu/g for Y0 to Y15, respectively. Furthermore, a similar pattern was observed in the remanent magnetization values, which increased upon partial substitution of Fe^{3+} with Y^{3+} ions. The remanent magnetization values were 32.75, 34.06, 31.53, and 30.51 emu/g for Y0 to Y15, in sequence. The trend of increasing followed by decreasing magnetization values may be attributed to high-temperature sintering (> 1,000 °C) and structural distortion caused by cation substitution of Fe^{3+} with Y^{3+} [2,20]. Mechanistically, each Fe^{3+} ion in a single unit cell of M-type hexaferrites occupies 5 crystallographic sites, including 1 trigonal bipyramidal site (2b), 1 tetrahedral site (4f1), and 3 octahedral sites (2a, 12k and $4f_2$) [11]. Moreover, it is known that 16 Fe^{3+} ions have spins aligned parallel to the c-axis of the crystal (forming the majority spin direction ↑ at sites 12k, 2a and 2b), while 8 Fe^{3+} ions are oriented in the opposite direction (forming the minority spin direction ↓ at sites $4f_1$ and $4f_2$) [19,50]. After the cancellation of the opposing magnetic moments between upward and downward spins of Fe^{3+} ions, a net magnetization results from 4 Fe^{3+} ions with upward spins. Therefore, it is understood that the substitution of Fe^{3+} with Y^{3+} ions at x = 0.05 tends to occupy the minority spin sites ↓ ($4f_1$ and $4f_2$), resulting in an increase in the M_{max} value in the Y5 sample [50,51]. On the other hand, in the Y10 and Y15 samples, it is suspected that some Fe^{3+} ions are removed from the majority spin sites, leading to a reduction in both maximum and remanent magnetization values [2,9,52].

The M-H loop curves of the Y0-Y15 samples measured under a maximum magnetic field of 10 kOe do not exhibit saturation. To gain a more detailed understanding of the magnetic properties, such as saturation magnetization, effective magnetocrystalline anisotropy constant and anisotropy field, these parameters can be calculated using the Law of Approach to Saturation (LAS) method. The LAS approach is defined as follows [33,53]:

$$M = M_S\left(1 - \frac{A}{H} - \frac{B}{H^2}\right) + \chi H \quad (3)$$

$$B = \frac{4K_{eff}^2}{15M_S^2} \quad (4)$$

$$H_a = \frac{2K_{eff}}{M_S} \text{ et} \quad (5)$$

where M_S is the saturation magnetization, A is a constant associated with material inhomogeneities, B is a constant related to magnetocrystalline anisotropy, H is the applied magnetic field, and χ is the magnetic susceptibility of the material. It is known that the χH term is considered significant only at high temperatures and high magnetic fields. Therefore, for samples measured at room temperature, this term can be neglected due to its negligible effect. As a result, Eq. (3) is simplified to Eq. (6). Furthermore, the estimation of the magnetic moment of the $BaFe_{12-x}Y_xO_{19}$ compounds can be obtained using Eq. (7), where M_W represents the molecular weight [2,53].

$$M = M_S\left(1 - \frac{B}{H^2}\right) \quad (6)$$

$$n_B\,(\mu_B) = \frac{M_W \times M_S}{5585} \quad (7)$$

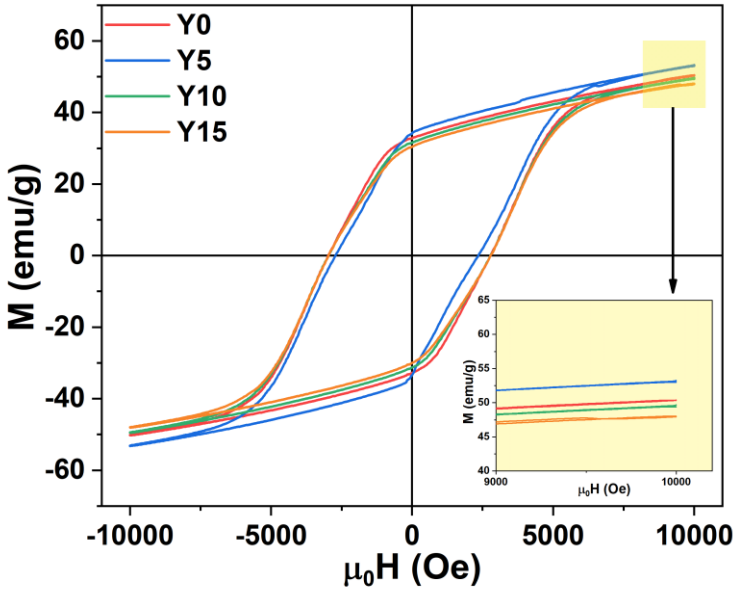

Figure 6 M-H loop curves of $BaFe_{12-x}Y_xO_{19}$ compounds (x = 0.0, 0.05, 0.10 and 0.15) measured at room temperature. The magnetization peaks for all samples are magnified in the inset.

The LAS method approach was applied to the M-H loops of all samples, as shown in **Figure 7**. Based on the fitted curves in the figure, several magnetic parameters were obtained, including saturation magnetization, effective magnetocrystalline anisotropy constant (K_{eff}) , anisotropy field (H_a), and magnetic moment (n_B), which are summarized in **Table 4** and compared with previous studies. Variations in the K_{eff} and H_a values were observed as the substitution of Fe^{3+} cations with Y^{3+} ions increased, showing a general decreasing trend. A high K_{eff} value indicates that the material exhibits hard magnetic characteristics, while a low K_{eff} value suggests soft magnetic behavior [53]. The effective anisotropy constant K_{eff} is influenced by particle size effects on the surface and size limitations. As the particle size decreases, the surface to volume ratio increases, leading to a greater contribution from surface anisotropy. This anisotropy arises due to the different bonding environments experienced by atoms at the surface compared to those in the bulk of the material. As a result, smaller particles tend to exhibit higher K_{eff} values. Conversely, in larger particles, K_{eff} is more strongly affected by the intrinsic properties of the material and its crystal structure [53]. Meanwhile, the obtained H_a values tend to decrease with increasing substitution of Fe^{3+} by Y^{3+}, which may be associated with the reduction in magnetocrystalline anisotropy of the material [42]. Furthermore, the magnetic moment values remained relatively stable, as summarized in **Table 4**.

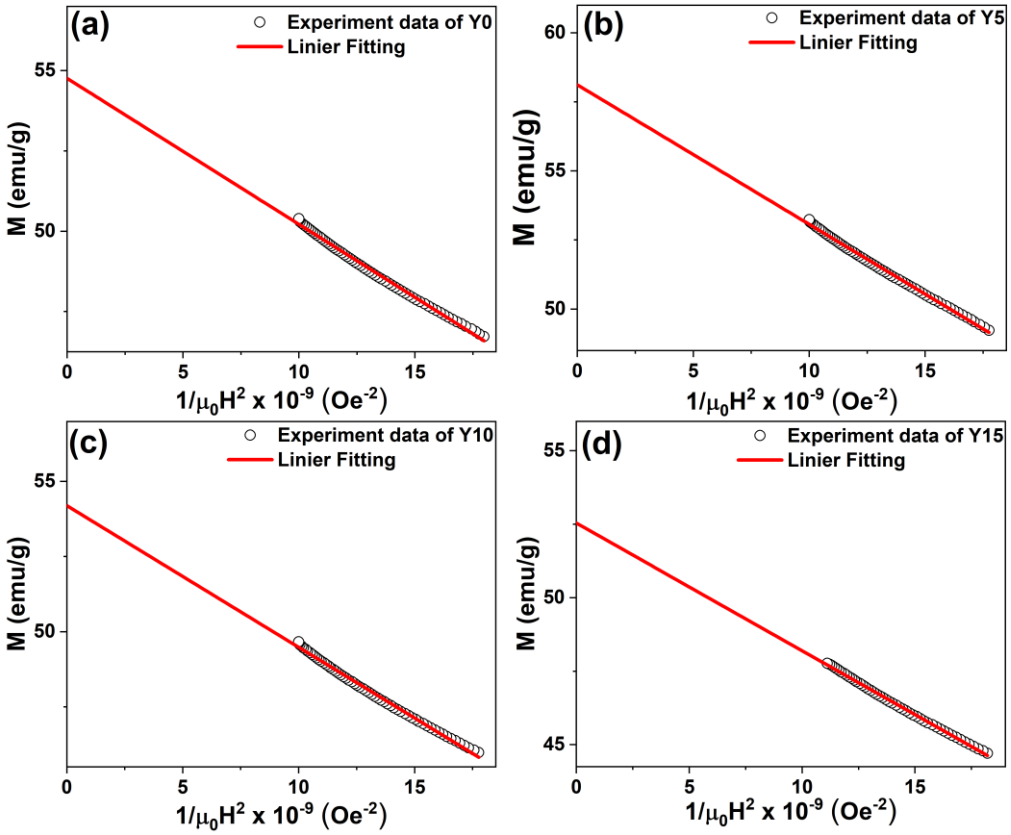

Figure 7 Plot of magnetization as a function of $1/1/H^2$ for $BaFe_{12-x}Y_xO_{19}$ (a) x = 0.0, (b) x = 0.05, (c) x = 0.1, and (d) x = 0.15 compounds.

Based on **Table 3**, the optimal $BaFe_{12-x}Y_xO_{19}$ composition for microwave absorber applications should exhibit low coercivity and high saturation magnetization. These characteristics are crucial because low coercivity allows the material to respond easily to an external magnetic field, while high saturation magnetization enhances the efficiency of electromagnetic wave absorption. In this study, the sample with x = 0.05 (Y5) demonstrated the best combination of these 2 parameters, making it a superior candidate compared to the other samples. Compared to previous studies, the Y5 sample exhibited competitive magnetic properties. Sarker *et al.* [2] synthesized $BaFe_{11.8}Y_{0.2}O_{19}$ via the sol-gel method and reported a high saturation magnetization (Ms) of 106.0 emu/g and coercivity (Hc) of 2389 Oe. Using the co-precipitation method, Ginting *et al.* [6] obtained Ms = 34.83 emu/g and Hc = 2099 Oe for $BaFe_8Co_2Ni_2O_{19}$. Meanwhile, Rehman *et al.* [24], through a solid-state reaction method, achieved Ms = 57.14 emu/g and Hc = 2,165 Oe for $Ba_{1-x}Y_xFe_{12}O_{19}$ with x = 0.05. In comparison, the Y5 sample in this study, synthesized using High Energy Milling, achieved Ms = 58.11 emu/g and Hc = 2,715 Oe.

Although the coercivity was slightly higher than that reported in Rehman *et al.* [24], the Y5 sample offers a favorable trade-off between magnetization strength and coercive field, which is critical for microwave absorption performance. This result highlights the potential advantage of the HEM technique in producing materials with improved microstructural uniformity and magnetic homogeneity. Accordingly, the $BaFe_{11.95}Y_{0.05}O_{19}$ composition can be considered a promising candidate for high-performance microwave absorbing materials.

Table 3 Magnetic variables of $BaFe_{12-x}Y_xO_{19}$ (x = 0.0, 0.05, 0.1 and 0.15).

Sample	Synthesis method	$\mu_0 H$ (kOe)	M_{max} (emu/g)	M_r (emu/g)	H_C (Oe)	Reference
Y0	HEM	10	50.39	32.75	2,933	**This work**
Y5	HEM	10	53.23	34.06	2,715	**This work**
Y10	HEM	10	49.65	31.53	2,942	**This work**
Y15	HEM	10	47.95	30.51	2,962	**This work**
$BaFe_{12}O_{19}$	**CP**	**20**	**32.02**	**16.98**	**6,958**	[6]
$BaFe_{10}Co_1Ni_1O_{19}$	**CP**	**20**	**34.34**	**17.31**	**4,233**	[6]
$BaFe_8Co_2Ni_2O_{19}$	**CP**	**20**	**34.83**	**18.03**	**2,099**	[6]
$BaFe_{12}O_{19}$	**SG**	**20**	**70.07**	**35.75**	**2,936**	[2]
$BaFe_{11.8}Y_{0.2}O_{19}$	**SG**	**20**	**100.27**	**49.86**	**2,389**	[2]
$BaFe_{11.6}Y_{0.4}O_{19}$	**SG**	**20**	**81.27**	**41.78**	**3,341**	[2]
$BaFe_{11.4}Y_{0.6}O_{19}$	**SG**	**20**	**82.95**	**41.78**	**2,923**	[2]
$BaFe_{12}O_{19}$	**SG**	**15**	**96**	**25.04**	**3,860**	[20]
$BaFe_{11.7}Y_{0.3}O_{19}$	**SG**	**15**	**96.70**	**51.62**	**3,150**	[20]
$BaFe_{11.5}Y_{0.5}O_{19}$	**SG**	**15**	**71.21**	**37.77**	**3,040**	[20]
$BaFe_{11.3}Y_{0.7}O_{19}$	**SG**	**15**	**63.31**	**34.04**	**3,400**	[20]
$BaFe_{11.1}Y_{0.9}O_{19}$	**SG**	**15**	**55.71**	**30.33**	**2,900**	[20]

Table 4 Magnetic variables of $BaFe_{12-x}Y_xO_{19}$ (x = 0.0, 0.05, 0.1 and 0.15) approaching by LAS method.

Sample	M_S *(emu/g)*	M_r/M_S	n_B (μ_B)	$K_{eff}\times10^6$	$H_a\times104$ *(emu/g)*	*B* (10^8)
Y0	54.75	0.649	10.89	2.25	8.25	4.54
Y5	58.11	0.639	11.56	2.52	8.70	5.04
Y10	54.19	0.634	10.78	2.28	8.40	4.71
Y15	52.53	0.636	10.45	2.12	8.07	4.34

Conclusions

The results of this study indicate that the addition of Yttrium (Y) as a dopant in barium hexaferrite ($BaFe_{12-x}Y_xO_{19}$) significantly affects the microstructure and magnetic properties of the material. The incorporation of Y leads to an increase in lattice parameters, shifts in XRD diffraction peaks, and a reduction in grain size, which in turn impacts the magnetic characteristics. Magnetic measurements reveal that the sample with x = 0.05 (Y5) exhibits the best performance, with the highest saturation magnetization (58.11 emu/g) and optimal coercive field (2,715 Oe). Therefore, Yttrium doping has proven effective in enhancing the magnetic properties of this material, making it a promising candidate for microwave absorber applications and other electromagnetic technologies.

Acknowledgements

The author would like to express sincere gratitude to the Graduate School of Universitas Sumatera Utara (USU), Indonesia for the support and facilities provided throughout the research process. Special thanks are also extended to the Research Center for Advanced Physics and Materials (PRMM) - BRIN for the technical assistance, laboratory facilities, and valuable scientific guidance during the implementation of this research.

Declaration of Generative AI in Scientific Writing

During the preparation of this work the authors used ChatGPT-4.0 in order to improving clarity and language quality. All scientific content, interpretation, and conclusions were developed independently by the authors. After using this tool/service, the authors reviewed and edited the content as needed and takes full responsibility for the content of the publication.

CRediT author statement

Nazaruddin Nasution: Conceptualization, Writing - original draft, Writing - review & editing, Investigation, Formal analysis. **Syahrul Humaidi:** Writing - review & editing, Formal analysis, Supervision. **Erna Frida:** Writing - review & editing, Investigation. **Marzuki Naibaho:** Writing - review & editing, Methodology, Resources, Data curation, Investigation, Formal analysis. **Phahul Zhemas Zul Nehan:** Writing - review & editing, Software, Investigation, Formal analysis, and Data Curation. **Masno Ginting:** Writing - review & editing, Formal Analysis, Validation, Supervision. **Tulus Na Duma:** Writing - review & editing, Investigation.

References

[1] Y Huang, Z Zhang, W Xing, T Xu, D Zhao, W Yang, J Lin, K Shi, J Li and Z Zhou. Enhanced polarization loss toward lanthanum-samarium doping-encoded defect genes of ferrite for optimizing microwave absorption. *ACS Applied Nano Materials* 2024; **7(10)**, 11146-11158.

[2] MSI Sarker, U Salma, MNI Khan, MM Rahman and MKR Khan. Impact of annealing temperature on the structural, magnetic and dielectric properties of $BaFe_{12-x}Y_xO_{19}$ (x = 0.0, 0.2, 0.4, 0.6) nanocrystalline samples. *Ceramics International* 2024; **50(22)**, 45868-45879.

[3] PZZ Nehan, O Vitayaya, DR Munazat, MTE Manawan, D Darminto and B Kurniawan. The magnetocaloric effect properties for potential applications of magnetic refrigerator technology: A review. *Physical Chemistry Chemical Physics* 2024; **26(20)**, 14476-14504.

[4] S Sharma, SR Parne, SSS Panda and S Gandi. Progress in microwave absorbing materials: A critical review. *Advances in Colloid and Interface Science* 2024; **327**, 103143.

[5] J Edianta, N Fauzi, M Naibaho, FS Arsyad and I Royani. Review of the effectiveness of plant media extracts in barium hexaferrite magnets ($BaFe_{12}O_{19}$). *Science and Technology Indonesia* 2021; **6(2)**, 39-52.

[6] M Ginting, P Sebayang, M Rianna, M Situmorang, H Fujiati, AP Tetuko, EA Setiadi, C Kurniawan and AMS Sebayang. Effect of Co and Ni additions as doping materials on the micro-structures and the magnetic properties of barium hexa-ferrites. *Case Studies in Thermal Engineering* 2020; **18**, 100589.

[7] G Gultom, M Rianna, P Sebayang and M Ginting. The effect of Mg-Al binary doped barium hexaferrite for enhanced microwave absorption performance. *Case Studies in Thermal Engineering* 2020; **18**, 100580.

[8] M Rianna, T Sembiring, M Situmorang, AP Tetuko, EA Setiadi, M Ginting and P Sebayang. Micro-structures and magnetic properties of Mg-Al substituted in barium hexa-ferrite prepared by co-precipitation method. *IOP Conference Series: Materials Science and Engineering* 2020; **725(1)**, 012049.

[9] R Topkaya, I Auwal and A Baykal. Effect of temperature on magnetic properties of $BaY_xFe_{12-x}O_{19}$ hexaferrites. *Ceramics International* 2016; **42(14)**, 16296-16302.

[10] R Topkaya. Effect of composition and temperature on the magnetic properties of $BaBi_xLa_xFe_{(12-2x)}O_{19}$ ($0.0 \leq x \leq 0.2$) hexaferrites. *Applied Physics A* 2017; **123(7)**, 488.

[11] H Basma, HT Rahal and R Awad. Enhancement of the magnetic properties of $Ba_{1-x}Bi_xFe_{12}O_{19}$ nanoparticles. *Journal of Magnetism and Magnetic Materials* 2021; **539**, 168413.

[12] M Naibaho, J Widakdo, B Kurniawan, PZZ Nehan, O Vitayaya, Novita, Ramlan, WA Adi and M Ginting. Analysis of structure, morphology, magnetic properties, and microwave absorption of *Lanthanum orthoferrite* ($LaFeO_3$). *Science and Technology Indonesia* 2024; **9(4)**, 851-856.

[13] R Topkaya. Effect of Zn substitution on temperature dependent magnetic properties of

$BaFe_{12}O_{19}$ hexaferrites. *Journal of Alloys and Compounds* 2017; **725**, 1230-1237.

[14] PD Thang, TA Ho, NT Dang, BW Lee, TL Phan, TV Manh, DH Kim and DS Yang. Mn-doped $(Ba,Y)Fe_{12}O_{19}$ hexaferrites: Crystal structure and oxidation states of Mn and Fe. *Current Applied Physics* 2020; **20(11)**, 1263-1267.

[15] MS Sihotang, MA Angelo, M Naibaho, M Maulidita, N Ichsan and M Ginting. Effect of barium hexaferrite doped yttrium (Y^{3+}) on the microwave absorption by solid-state reaction methods. *Journal of Technomaterial Physics* 2025; **7(1)**, 063-070.

[16] C Kaew-On, J Yuennan, N Tohluebaji, P Channuie, S Ruangdit, R Samran, T Tochomphoo and R Siri. Enhanced hydrophobicity, thermal stability, and x-ray shielding efficiency of $BaSO_4$/P(VDF-HFP) nanocomposites for advanced lead-free radiation protection. *Polymers* 2025; **17(6)**, 723.

[17] J Yuennan, N Muensit, N Tohluebaji, W Chailad, L Yang, N Sukhawipat, GA Ashraf and P Channuie. Tailoring dielectric properties and crystallinity in poly(vinylidene fluoride-co-hexafluoropropylene) nanocomposites via iron (III) chloride hexahydrate incorporation. *Scientific Reports* 2025; **15(1)**, 17810.

[18] PD Thang, NH Tiep, TA Ho, ND Co, NTM Hong, QV Dong, BW Lee, TL Phan, NT Dang, DT Khan and DS Yang. Electronic structure and multiferroic properties of (Y, Mn)-doped barium hexaferrite compounds. *Journal of Alloys and Compounds* 2021; **867**, 158794.

[19] A Baykal, IA Auwal, S Güner and H Sözeri. Magnetic and optical properties of Zn^{2+} ion substituted barium hexaferrites. *Journal of Magnetism and Magnetic Materials* 2017; **430**, 29-35.

[20] N Thakur, I Sharma, P Thakur, M Mahajan, S Bhardwaj, R Jasrotia, A Dahshan, HI Elsaeedy, S Kaur, G Anand, P Sharma, KM Batoo and G Kumar. Improvement in the structural, magnetic and electromagnetic behaviour of barium hexaferrites with yttrium doping for EMI shielding. *Journal of Alloys and Compounds* 2024; **976**, 173042.

[21] X Liu, R Ji, M Yang, W Chen, H Chen, X Song, J Liu, M Zhang and L Zhang. Facilitating enhanced microwave absorption properties of barium hexaferrite/polyaniline composites based on tunable interfacial polarization by rare earth doping. *Journal of Alloys and Compounds* 2023; **937**, 168391.

[22] A Hashhash, A Hassen, WS Baleidy and HS Refai. Impact of rare-earth ions on the physical properties of hexaferrites $Ba_{0.5}Sr_{0.5}RE_{0.6}Fe_{11.4}O_{19}$, (RE = La, Yb, Sm, Gd, Er, Eu, and Dy). *Journal of Alloys and Compounds* 2021; **873**, 159812.

[23] GM Rai, MA Iqbal and KT Kubra. Effect of Ho^{3+} substitutions on the structural and magnetic properties of $BaFe_{12}O_{19}$ hexaferrites. *Journal of Alloys and Compounds* 2010; **495(1)**, 229-233.

[24] KMU Rehman, X Liu, M Li, S Jiang, Y Wu, C Zhang, C Liu, X Meng and H Li. Synthesization and magnetic properties of $Ba_{1-x}Y_xFe_{12}O_{19}$ hexaferrites prepared by solid-state reaction method. *Journal of Magnetism and Magnetic Materials* 2017; **426**, 183-187.

[25] I Sharma, T Kumari, N Thakur, P Sharma, KM Batoo and R Verma. Citrate precursor route for Y^{3+} substituted M-type Ba-hexaferrite: Synthesis, the effect of doping on structural, optical, magnetic and anti-bacterial properties. *Materials Chemistry and Physics* 2023; **302**, 127664.

[26] DT Rahardjo, S Budiawanti, S Suharno, R Suryana, A Supriyanto and B Purnama. Decreasing of magnetic saturation of yttrium doped cobalt ferrite prepared by the sol-gel auto-combustion. *Trends in Sciences* 2024; **21(4)**, 7320-7320.

[27] M Rianna, M Situmorang, C Kurniawan, AP Tetuko, EA Setiadi, M Ginting and P Sebayang. The effect of Mg-Al additive composition on microstructure, magnetic properties, and microwave absorption on $BaFe_{12-2x}Mg_xAl_xO_{19}$ (x = 0–0.5) material synthesized from natural iron sand. *Materials Letters* 2019; **256**, 126612.

[28] Z Mosleh, P Kameli, M Ranjbar and H Salamati. Effect of annealing temperature on structural and magnetic properties of $BaFe_{12}O_{19}$ hexaferrite nanoparticles. *Ceramics International* 2014; **40(5)**, 7279-7284.

[29] R Yensano and S Phokha. Effect of pH on single phase $BaFe_{12}O_{19}$ nanoparticles and their improved magnetic properties. *Journal of Materials Science: Materials in Electronics* 2020; **31(14)**, 11764-11773.

[30] S Güner, IA Auwal, A baykal and H Sözeri. Synthesis, characterization and magneto optical properties of $BaBi_xLa_xY_xFe_{12-3x}O_{19}$ ($0.0 \leq x \leq 0.33$) hexaferrites. *Journal of Magnetism and Magnetic Materials* 2016; **416**, 261-268.

[31] II Sharma, N Thakur, M Mahajan, R Jasrotia, G Anand, R Neffati, A Dahshan, HI Elsaeedy, P Sharma and G Kumar. Electrospun Y^{3+}-modified $BaFe_{12}O_{19}$hexaferrite-based nano-fibers with enhanced magnetic behavior for magnetic memory devices and permanent magnets. *Journal of Materials Science: Materials in Electronics* 2023; **34(33)**, 2180.

[32] VG Kostishin, VV Korovushkin, IM Isaev, AY Mironovich, SV Trukhanov, VA Turchenko, KA Astapovich and AV Trukhanov. Features of the cation distribution and magnetic properties of $BaFe_{12-x}Y_xO_{19}$ hexaferrites. *Physics of the Solid State* 2021; **63(2)**, 253-260.

[33] Y Chen, Y Wang, Y Liu, Q Liu, C Wu, B Qi and H Zhang. Microstructure and magnetic properties of Y substituted M-type hexaferrite $BaY_xFe_{12-x}O_{19}$. *Journal of Materials Science: Materials in Electronics* 2019; **30(6)**, 5911-5916.

[34] IA Auwal, B Ünal, A Baykal, U Kurtan, MD Amir, A Yıldız and M Sertkol. Electrical and dielectric properties of Y^{3+}-substituted barium hexaferrites. *Journal of Superconductivity and Novel Magnetism* 2017; **30(7)**, 1813-1826.

[35] TR Wagner. Preparation and crystal structure analysis of magnetoplumbite-type $BaGa_{12}O_{19}$. *Journal of Solid State Chemistry* 1998; **136(1)**, 120-124.

[36] V Anbarasu, PM Md Gazzali, T Karthik, A Manigandan and K Sivakumar. Effect of divalent cation substitution in the magnetoplumbite structured $BaFe_{12}O_{19}$ system. *Journal of Materials Science: Materials in Electronics* 2013; **24(3)**, 916-926.

[37] MA Almessiere, Y Slimani, NA Tashkandi, A Baykal, MF Saraç, AV Trukhanov, Ercan, Belenli and B Ozçelik. The effect of Nb substitution on magnetic properties of $BaFe_{12}O_{19}$ nanohexaferrites. *Ceramics International* 2019; **45(2)**, 1691-1697.

[38] Y Marouani, J Massoudi, M Noumi, A Benali, E Dhahri, P Sanguino, MPF Graça, MA Valente and BFO Costa. Electrical conductivity and dielectric properties of Sr doped M-type barium hexaferrite $BaFe_{12}O_{19}$. *RSC Advances* 2021; **11(3)**, 1531-1542.

[39] A Pathania, S Bhardwaj, SS Thakur, JL Mattei, P Queffelec, LV Panina, P Thakur and A Thakur. Investigation of structural, optical, magnetic and electrical properties of tungsten doped Ni-Zn nano-ferrites. *Physica B Condensed Matter* 2018; **531**, 45-50.

[40] KM Batoo, M Hadi, R Verma, A Chauhan, R Kumar, M Singh and OM Aldossary. Improved microwave absorption and EMI shielding properties of Ba-doped Co-Zn ferrite. *Ceramics International* 2022; **48(3)**, 3328-3343.

[41] PZZ Nehan, B Kurniawan, DR Munazat, O Vitayaya, M Naibaho, T Sudiro, MTE Manawan, D Darminto and H Nojiri. Calciumion deficiency and its influence on structure, critical behavior, magnetic and magnetocaloric effect properties in $La_{0.7}Ca_{0.2-x}\square_xSr_{0.1}MnO_3$ ($x = 0.00$, 0.05, and 0.10) manganites. *Journal of Alloys and Compounds* 2025; **1020**, 179467.

[42] IA Auwal, H Güngüneş, S Güner, SE Shirsath, M Sertkol and A Baykal. Structural, magneto-optical properties and cation distribution of $SrBi_xLa_xY_xFe_{12-3x}O_{19}$ ($0.0 \leq x \leq 0.33$) hexaferrites. *Materials Research Bulletin* 2016; **80**, 263-272.

[43] BK Rai, SR Mishra, VV Nguyen and JP Liu. Synthesis and characterization of high coercivity rare-earth ion doped $Sr_{0.9}RE_{0.1}Fe_{10}Al_2O_{19}$ (RE: Y, La, Ce, Pr, Nd, Sm, and Gd). *Journal of Alloys and Compounds* 2013; **550**, 198-203.

[44] G Kishor, RN Bhowmik, RJ Choudhary, S Chakravarty and R Venkatesh. Development of highly oriented crystals in the magnetoplumbite structure of metal (Sr, Cr, Sc) doped M-type $BaFe_{12}O_{19}$ hexaferrite films with improved optical and magnetic properties. *Journal of Alloys and Compounds* 2024; **1009**, 176896.

[45] M Sharma, SC Kashyap and HC Gupta. Effect of Mg-Zr substitution and microwave processing on

magnetic properties of barium hexaferrite. *Physica B Condens Matter* 2024; **448**, 24-28.

[46] PT Tho, N Tran, NQ Tuan, TA Ho, CTA Xuan, HN Toan and BW Lee. Detailed microwave loss mechanisms for nanocomposites of La-doped $BaFe_{12}O_{19}$ and polyaniline. *Ceramics International* 2023; **49**, 23669-23679.

[47] N Tran, MY Lee, WH Jeong, TL Phan, NQ Tuan and BW Lee. Thickness independent microwave absorption performance of La-doped $BaFe_{12}O_{19}$ and polyaniline composites. *Journal of Magnetism and Magnetic Materials* 2021; **538**, 168299.

[48] P Sinuhaji, M Ginting, P Sebayang, M Rianna, M Hamid, TR Simbolon, V Harahap, AP Tetuko, EA Setiadi, NS Asri, LF Nurdiyansah and AMS Sebayang. Microstructures, magnetic and electrical properties of $BaFe_{12}O_{19}$/ZnO composite material. *International Journal of Electrochemical Science* 2021; **16(8)**, 210831.

[49] B Soerya, A Fachredzy, M Naibaho and M Ginting. Effect of silicon rubber (SIR) in fabrication of NdFeB/$BaFe_{12}O_{19}$-based hybrid magnet. *Indonesian Physical Review* 2024; **7(1)**, 32-38.

[50] MR Islam, MKR Khan, MS Hossain, MM Rahman, MM Haque, M Aliuzzaman, MK Alam and MSI Sarker. Structural, thermodynamic, and magnetic properties of $SrFe_{12}O_{19}$ hexaferrite modified by co-substitution of Cu and Gd. *RSC Advances* 2024; **14(11)**, 7314-7328.

[51] PN Anantharamaiah, NS Chandra, HM Shashanka, R Kumar and B Sahoo. Magnetic and catalytic properties of Cu-substituted $SrFe_{12}O_{19}$ synthesized by tartrate-gel method. *Advanced Powder Technology* 2020; **31(6)**, 2385-2393.

[52] SK Chawla, RK Mudsainiyan, SS Meena and SM Yusuf. Sol-gel synthesis, structural and magnetic properties of nanoscale M-type barium hexaferrites $BaCo_xZr_xFe_{(12-2x)}O_{19}$. *Journal of Magnetism and Magnetic Materials* 2014; **350**, 23-29.

[53] SK Yadav, DP Pabba, A Soosairaj, K Divya, LR Asirvatham, VS Manikandan, M Navaneethan and A Thirumurugan. Study on the structural, magnetic, and magnetodielectric properties of M-type $BaFe_{12}O_{19}$ and $SrFe_{12}O_{19}$ hexaferrite nanoparticles. *Surfaces and Interfaces* 2024; **52**, 104956.